CHALMERS
UNIVERSITY OF TECHNOLOGY

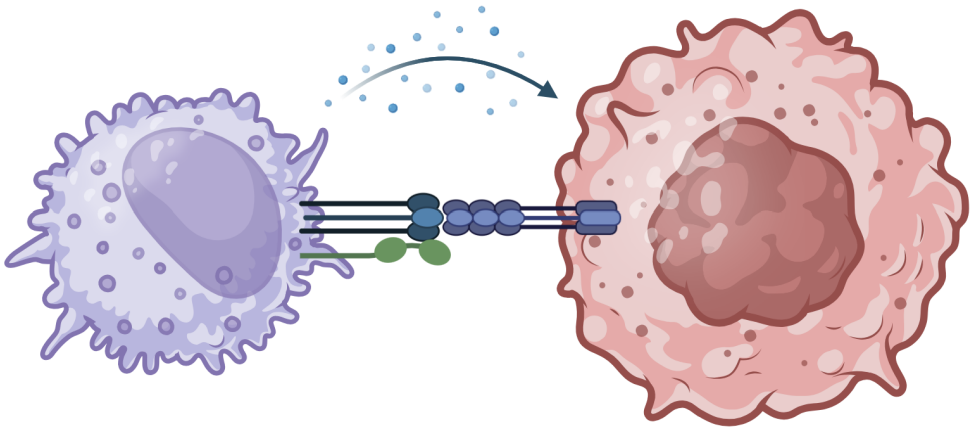

The Role of TRAIL and TRAIL receptors in NKp46-Mediated Cytotoxicity Against ER-Stressed Cancer Cells

Master's Thesis Project in Biotechnology

WILLIAM LAGER

DEPARTMENT OF LIFE SCIENCES
CHALMERS UNIVERSITY OF TECHNOLOGY
Gothenburg, Sweden 2026
www.chalmers.se

Degree project report 2026

The Role of TRAIL and TRAIL-Receptors in NKp46-mediated Cytotoxicity Against ER-stressed Cancer Cells

WILLIAM LAGER

CHALMERS
UNIVERSITY OF TECHNOLOGY

Department of Life Sciences
Chalmers University of Technology
Gothenburg, Sweden 2026

The Role of TRAIL and TRAIL- Receptors in NKp46-mediated Cytotoxicity Against ER-stressed Cancer Cells
WILLIAM LAGER

Supervisor: Fredrik Bergh Thorén, University of Gothenburg, Department of Medical Biochemistry and Cell biology
Examiner: Anna Karlsson-Bengtsson, Chalmers, Department of Life Sciences

60 Credits Master's Thesis 2026
Department of Life Sciences
Chalmers University of Technology
SE-412 96 Gothenburg
Sweden
Telephone +46 31 772 1000

Cover: NK cell expressing NKp46 and TRAIL binding to TRAIL-receptors on a cancer cell. The image was generated with OpenAI ChatGPT (GPT-5.5) and modified in Biorender.

Typeset in LaTeX
Gothenburg, Sweden 2026

The Role of TRAIL and TRAIL receptors in NKp46-Mediated Cytotoxicity Against ER-Stressed Cancer Cells

WILLIAM LAGER
Department of Life Sciences
Chalmers University of Technology

Abstract

Natural killer (NK) cells play a critical role in anti-tumor immunity through the recognition and elimination of malignant cells. The activating receptor NKp46 has been implicated in cytotoxicity of many cancer targets, but the molecular mechanisms underlying this process remain incompletely understood. Previous studies have proposed ER-stress induced ecto-calreticulin (ecto-CRT) as a ligand for NKp46, whereas more recent evidence suggests that NKp46 recognizes TRAIL receptors through *in cis* interaction with membrane-bound TRAIL. The aim of this thesis was to elucidate the molecular mechanisms by which TRAIL and TRAIL receptors contribute to NKp46-mediated recognition and killing of ER-stressed cancer cells and to identify structural determinants of the NKp46–TRAIL interaction. ER stress and immunogenic cell death were induced in cancer cell lines using anthracyclines and oxaliplatin. NK-cell responses were assessed using degranulation assays in combination with NKp46 blockade, *TNFSF10* (TRAIL) knockdown, and CRT blockade. In parallel, AlphaFold-generated structural models of the NKp46–TRAIL complex were analyzed using computational alanine scanning and binding-energy calculations, in order to identify key interaction determinants. Immunogenic cell death-inducing treatments resulted in the co-upregulation of calreticulin and TRAIL receptors, particularly TRAIL-R2. Functional studies demonstrated that TRAIL was required for efficient NKp46-mediated degranulation against both untreated and ER-stressed cancer cells. NKp46 blockade and *TNFSF10* knockdown markedly reduced NK-cell activation, and the effect of NKp46 blockade was largely lost in the absence of TRAIL expression. In contrast, CRT blockade did not significantly impair NK-cell degranulation, suggesting that TRAIL receptor recognition constitutes the dominant mechanism of NKp46-dependent cytotoxicity under conditions where TRAIL is present. Complementary structural modeling of the NKp46–TRAIL complex identified recurrent energetic hotspot residues on NKp46, including Tyr 100 and Arg 70, although the low confidence of AlphaFold-predicted interfaces highlights the need for experimental validation. Together, these findings support a model in which TRAIL and TRAIL receptors mediate NKp46-dependent NK-cell recognition of ER-stressed cancer cells. The study provides mechanistic insight into NKp46-dependent tumor surveillance and identifies potential targets for engineering improved NK-cell receptor–ligand interactions for cancer immunotherapy.

Acknowledgements

I would like to express my sincere gratitude to my main supervisor, Fredrik Bergh Thorén, for his continuous guidance, support, and encouragement throughout the entire project. I am also deeply grateful to Chiara Badami for her invaluable help in the lab, her constant support and generously offering help whenever needed. My thanks also go to Erna Islamagic for her generous support and for always being approachable and willing to help. I would also like to thank Leif Eriksson and Sayyed Jalil Mahdizadeh for giving me the opportunity to explore molecular modelling as part of this project. I would further like to thank all members of TIMM lab for sharing their expertise, advice, and a supportive research environment throughout the entire project. I am grateful to my examiner, Anna Karlsson-Bengtsson, for her feedback and constructive input on the project. I would also like to acknowledge the Sahlgrenska Center for Cancer Research for providing the opportunity and facilities to carry out my thesis project. Finally, I would like to thank my family and friends for their unwavering support and encouragement outside of the project.

William Lager, Gothenburg, June 2026

List of Acronyms

Below is the list of acronyms that have been used throughout this thesis listed in alphabetical order:

CRT	Calreticulin
DAMP	Damage-associated molecular pattern
DC	Dendritic cell
eIF2	Eukaryotic initiation factor 2
ER	Endoplasmic reticulum
ERAD	ER-associated protein degradation
HLA	Human leukocyte antigen
HMGB1	Non-histone nuclear protein high-mobility group box 1
ICD	Immunogenic cell death
Ig	Immunoglobulin
ipTM	Interface predicted template modeling (score)
IRE1	Inositol-requiring enzyme-1
ITAM	Immunoreceptor tyrosine-based activation motif
ITIM	Immunoreceptor tyrosine-based inhibitory motif
KIR	Killer immunoglobulin-like receptor
MD	Molecular dynamics
MHC	Major histocompatibility complex
SNARE	Soluble *N*-ethylmaleimide-sensitive factor attachment protein receptor
MM-GBSA	Molecular mechanics generalized born surface area
NCR	Natural cytotoxicity receptor
PERK	PKR-like endoplasmic reticulum kinase
PKR	Protein kinase R
PLC	Peptide loading complex
pTM	Predicted template modeling (score)
TNF	Tumor necrosis factor
TRAIL	TNF-related apoptosis-inducing ligand
TRAIL-R	TRAIL-receptor
UPR	Unfolded protein response

Contents

List of Figures

List of Tables

1

Introduction

1.1 Background

1.1.1 Natural killer cells in immune surveillance

Natural killer (NK) cells are cytotoxic lymphocytes that play a central role in the innate immune response by targeting and eliminating infected, transformed, and stressed cells without the need for prior antigen sensitization [1]. This is in contrast to cytotoxic T-lymphocytes whose activation is largely dependent on antigen presentation by dendritic cells. Instead, the activation of NK cells is tightly regulated by a repertoire of germline-encoded activating and inhibitory surface receptors. Specifically, inhibitory receptors such as killer immunoglobulin-like receptors (KIRs) and NKG2A/CD94 provide NK cells with inhibitory signals through recognition of human leukocyte antigen (HLA) class I molecules and the non-classical HLA-E, respectively, which are typically expressed on healthy nucleated cells but are frequently downregulated in tumor or virus-infected cells. In contrast, activating receptors such as NKG2D and the natural cytotoxicity receptors (NCRs), recognize ligands that are commonly induced or upregulated on the surface of stressed, transformed, or senescent cells. The main functions of NK cells are summarized in Figure 1.1.

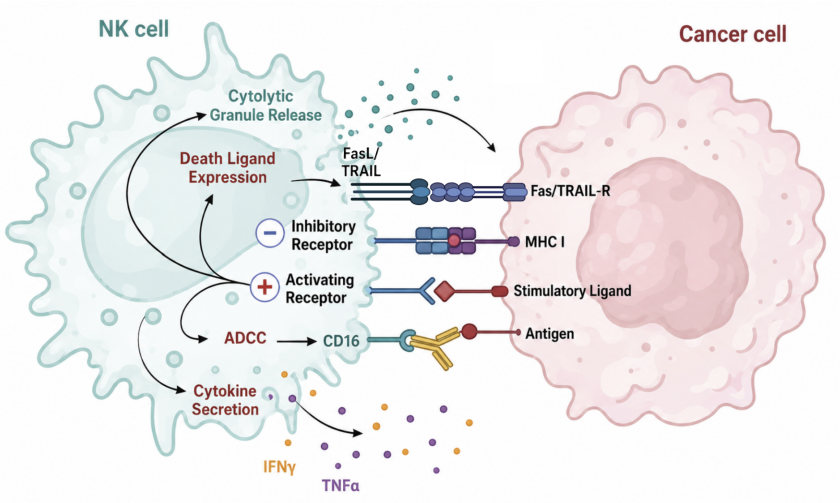

Figure 1.1: Overview of the main functions of NK cells. The illustration shows NK cell contact with a cancer cell. The image was generated using OpenAI ChatGPT (GPT-5.5).

Similar to T cells, there are two primary ways in which NK cells induce apoptosis in target cells. They can either release cytotoxic granules containing granzyme B, or they can use membrane-bound ligands that engage death receptors, initiating caspase cascades, eventually leading to apoptosis in the target cell [2]. Death ligands

such as FasL and tumor necrosis factor (TNF)-related apoptosis inducing ligand (TRAIL), expressed on the NK cell surface engage death receptors CD95/Fas and TRAIL-R1/2 (also called DR4/5), respectively, on the surface of the target cell. Interestingly, it has been shown that NK cells gradually switch from granzyme B to death receptor-mediated cytotoxicity during so-called serial killing, during which a single activated NK cell sequentially identifies, and destroys multiple target cells [2]. In addition to mediating direct cytotoxicity, activated NK cells secrete pro-inflammatory cytokines such as interferon-γ (IFN-γ) and TNF-α, which contribute to immune regulation and promote the activation of other innate and adaptive immune cells [1].

1.1.2 NKp46: a central activating receptor of NK cells

Among activating NK-cell receptors, the NCRs are particularly important for initiating NK cell-mediated responses. In humans, the NCR family consists of three receptors: NKp30, NKp44, and NKp46. Of these, NKp30 and NKp46 are constitutively expressed on both resting and activated NK cells, whereas NKp44 is induced only following cytokine-mediated activation [3][4]. NKp46 is a type I transmembrane protein and consists of two immunoglobulin (Ig)-like extracellular domians (D1 and D2) connected by an interdomain hinge, followed by an approximately 40-residue stalk region, a transmembrane domain, and a short cytoplasmic tail [5] [6]. A positively charged residue in the transmembane region allows the receptor to associate with the immunoreceptor tyrosine-based activation motif (ITAM)-containing FcRIγ and CD3ζ (Fig. 1.2). The ITAM contains two tyrosines which are phosphorylated by Src kinase family members and form a binding site for Src homology 2 (SH2) domains of the tyrosine kinases ZAP70 and Syk, mediating the signal inside the NK cell [1].

NKp46 is important for killing of many cancer targets [7]. Despite its importance, the full spectrum of NKp46 ligands remains incompletely defined. Several pathogen-derived ligands have been identified, including viral haemagglutinins and fungal adhesins [1]. In addition, NKp46 has been reported to recognize vimentin expressed on host cells in response to *Mycobacterium tuberculosis* infection [1]. However, the endogenous ligands responsible for mediating NKp46-dependent recognition of cancer cells remain largely unknown. A recent paper found that NKp46 recognizes externalized calreticulin (ecto-CRT) on target cells in response to endoplasmic reticulum (ER) stress [8]. In contrast, unpublished data from the Thorén group indicate that NKp46 interacts with TRAIL *in cis* and forms an immunoreceptor complex that recognizes TRAIL receptors on target cells. Nevertheless, the mechanisms governing NKp46 ligand recognition and downstream cytotoxicity remain incompletely understood.

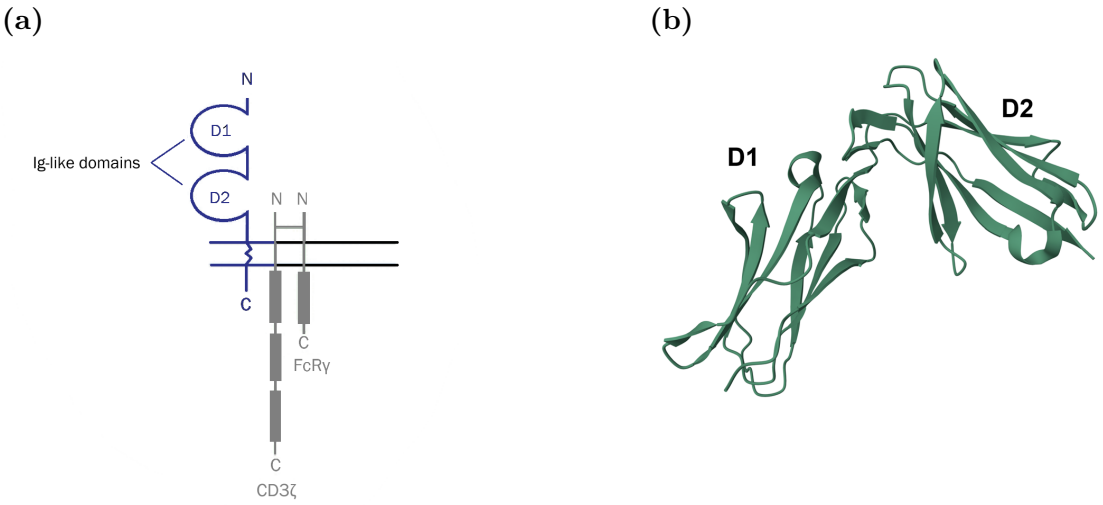

Figure 1.2: The structure of NKp46. (a) Schematic diagram of NKp46 with its two extracellular Ig-like domains connected by a hinge-region, a stalk region, and a transmembrane domain followed by a short cytoplasmic tail. Via a positively charged residue in the transmembrane domain, the receptor associates with the ITAM-containing adaptors FcRIγ and CD3ζ. (b) Crystal structure of the extracellular domain of NKp46 (PDB ID: 1P6F)

1.1.3 Cellular response to ER stress: the unfolded protein response

Endoplasmic reticulum (ER)-stress is characterized by accumulation of misfolded or unfolded proteins in the ER lumen, triggering a chain of pathways called the unfolded protein response (UPR) (Fig. 1.3). The UPR is mediated by three main sensors: protein kinase R (PKR)-like ER kinase (PERK), inositol-requiring enzyme 1 (IRE1), and activating transcription factor 6 (ATF6), which are normally maintained in an inactive state through association with the ER chaperone BiP [9]. Upon ER stress, BiP shows greater binding affinity for misfolded and unfolded proteins and therefore dissociates, enabling sensor activation and downstream signaling [10]. Initially, this adaptive signaling network aims to reduce protein load and enhance folding capacity via transcriptional reprogramming, mRNA decay, global protein translation attenuation, removal of misfolded proteins through the ER-associated protein degradatation (ERAD) system, as well as recycling of misfolded proteins via induction of autophagy [11][10]. Importantly, PERK activation induces rapid phosphorylation of eIF2α, leading to transient attenuation of global protein synthesis and reduced ER protein load. However, during excessive or prolonged ER stress, the UPR transitions from cytoprotective to pro-apoptotic, evenutally leading to cell death. Persistent ER stress is a common feature of many cancers. In tumor cells, rapid proliferation, hypoxia, nutrient deprivation, and high metabolic demand frequently disrupt ER homeostasis and promote chronic UPR activation.

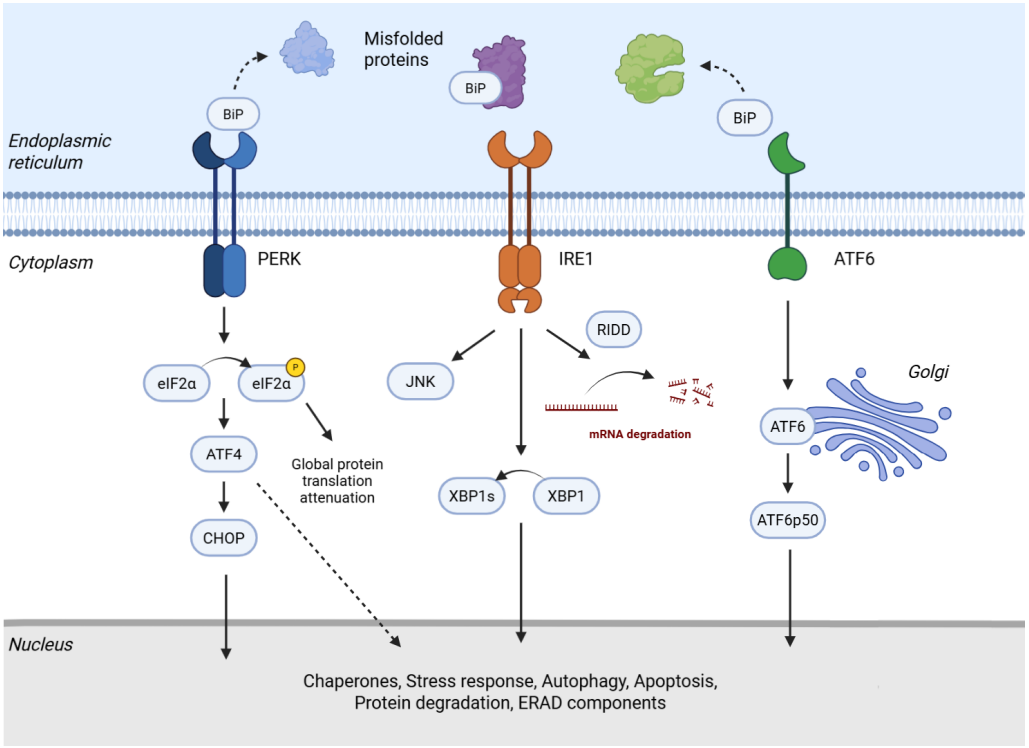

Figure 1.3: Summary of the main pathways that make up the unfolded protein response. The figure was created using Biorender.

1.1.4 Calreticulin: a hallmark of immunogenic cell death

Certain anticancer therapies, including anthracycline- and oxaliplatin-based chemotherapy, have been shown to induce particularly effective antitumor responses in immunocompetent compared with immunodeficient hosts [12], highlighting the contribution of adaptive immune responses to therapeutic efficacy. This is particularly well demonstrated when murine cancer cells are treated with anthracyclines or oxaliplatin *in vitro* followed by injection into syngenic mice in which they are able to provide long-term protection against subsequent exposure to cancer cells of the same type [13]. This phenomenon is referred to as immunogenic cell death (ICD), a form of regulated cell death capable of eliciting adaptive immune responses through the release or surface exposure of damage-associated molecular patterns (DAMPs). There are three distinct events involving DAMPs shown to be critical for the immunogenicity of cell death: (1) the pre-apoptotic exposure of CRT (ecto-CRT) on the cell surface, (2) the extracellular secretion of ATP, and (3) the release of non-histone nuclear protein high-mobility group box 1 (HMGB1) into the extracellular space following nuclear and plasma membrane permeabilization [12]. In particular, by binding receptors on dendritic cells (DCs), ecto-CRT serves as an "eat-me" signal, triggering the engulfment of cells that are potential sources of tumor-associated antigens.

Under physiological conditions, CRT is predominantly localized to the lumen of the endoplasmic reticulum, where it functions as a calcium-binding chaperone involved in protein folding and quality control [14]. Together with the oxidoreductase ERp57

and other protein components, CRT also forms part of the peptide-loading complex (PLC), responsible for assembly and peptide loading of major histocompatibility complex (MHC) class I molecules prior to their transport to the cell surface [15].

During ICD, surface exposure of CRT is accompanied by translocation of ERp57 to the plasma membrane. The exact molecular mechanism underlying the ICD-associated externalization of CRT/ERp57, has not yet been fully established. However, this process is known to involve ER stress and components of the unfolded protein response (UPR), particularly PERK-mediated phosphorylation of eIF2α (p-eIF2α). Indeed, disruption of PERK or expression of a non-phosphorylatable eIF2α mutant was shown to abolish CRT/ERp57 surface translocation without preventing cell death itself [16]. Accordingly, phosphorylation of eIF2α is frequently used as a biomarker of immunogenic cell death [17]. In addition, CRT/ERp57 externalization requires additional downstream apoptotic and vesicular trafficking processes including sub-apoptotic partial caspase-8 acitvation, activation of pro-apoptotic Bcl-2 family members Bax and Bak, anterograde ER-Golgi trafficking and SNARE-dependent exocytosis [16].

1.2 Aim and purpose

Among the activating NK cell receptors, the previously mentioned NCRs are particularly important for initiating NK cell-mediated responses. NKp46, a key activating NCR, is constitutively expressed on resting and activated NK cells and plays a crucial role in recognizing ligands on virus-infected and tumor cells [18]. Despite its importance, the full spectrum of NKp46 ligands remains incompletely defined. Although some pathogen products such as viral haemagglutinins and fungal adhesins have been identified as NKp46 ligands [1], the endogenous ligands for NKp46 are largely unknown. A recent paper found that NKp46 recognizes ecto-CRT on target cells in response to ER stress [8]. In contrast, unpublished data from the Thorén group indicates that NKp46 interacts with TRAIL *in cis* and forms an immunoreceptor complex that recognizes TRAIL receptors on target cells. Importantly, NKp46-mediated cytotoxicity appears to be not merely facilitated by, but actually dependent on, this mechanism as siRNA-mediated knockdown of TRAIL impairs NKp46-mediated cytotoxicity. Given that the reported affinity between NKp46 and CRT is approximately thousandfold lower than that of TRAIL binding to TRAIL receptors [8][19], it was hypothesized that TRAIL-mediated interactions may constitute the dominant mechanism underlying NKp46-dependent cytotoxicity. Interestingly, it has been shown that TRAIL interacts with CRT and associates with TRAIL-R1/2 in colocalization and immunoprecipitation experiments [20]. Nevertheless, the relationship among NKp46, CRT, TRAIL, and TRAIL-receptors in the context of ER stress remains to be fully elucidated. Therefore, the aim of this thesis project is to elucidate the molecular mechanisms by which TRAIL and TRAIL receptors contribute to NKp46-mediated recognition and killing of ER-stressed cancer cells. To complement the functional studies, structural modeling of NKp46–TRAIL interactions will be performed to identify key interacting residues and explore their structural context.

1.3 Specific objectives

To achieve the stated aim, the following objectives have been established: (1) To elucidate the role of TRAIL and TRAIL receptors in NKp46-mediated recognition and cytotoxicity of ER-stressed cancer cells, and (2) to characterize the structural basis of NKp46–TRAIL interactions using AI-based structure prediction and molecular modeling, and to identify key stabilizing residues within the TRAIL-NKp46 interface.

The first objective aims to address three questions: (1) *how* and *if* the importance of TRAIL-receptors changes when ER stress is induced in target cells, (2) whether the proposed NKp46 ligand ecto-CRT can trigger NKp46-mediated cytotoxicity independently of TRAIL and/or TRAIL-receptors, and (3) whether TRAIL-receptors are capable of mediating NKp46-dependent cytotoxicity in the absence of ecto-CRT under conditions of ER stress. To address these questions, ER stress was induced in target cells and NK cell degranulation and cytotoxicity assays was performed in combination with siRNA-mediated knockdown of the TRAIL-encoding gene, and/or blocking antibodies to select receptors/ligands.

The second objective aims to address the question of which molecular interactions that are critical for the formation and stability of the NKp46–TRAIL complex. To address these questions, AI-based structure prediction was employed to model the NKp46–TRAIL complex and identify its interaction interface, followed by *in silico* mutagenesis, binding free-energy calculations, and molecular dynamics simulations to evaluate the contribution of individual residues to complex stability and to assess the effects of selected mutations on binding affinity.

2

Methods

In this section, the general methods used in this project will be presented. Additional details and specific protocols can be found in Appendix.

2.1 Cell lines

JEG-3, A549, MDA-MB-231, and Jurkat cells were provided by the American Type Culture Collection (ATCC). Cell lines JEG-3 and MDA-MB-231 were cultured in DMEM (Gibco), A549 in Ham's F-12K Medium (Gibco), and Jurkat in RPMI (Gibco) at 37°C in 5% CO_2. All media were supplemented with 10% heat-inactivated FCS, and 1% penicillin-streptomycin (Gibco). To maintain subconfluency, adherent cells were continuously passaged using a trypsin–EDTA solution (0.25% trypsin (Thermo Fisher Scientific, cat. no. 15090046) and 0.5 mM EDTA (Thermo Fisher Scientific, cat. no. AM9260G) in PBS).

2.2 Induction of ER stress and immunogenic cell death

Cells were seeded in 6-well plates at a density of $2 \cdot 10^5$ cells per well 48 hours prior to treatment with either 2 µM doxorubicin (Sigma; cat. no. D1515) or 100 µM oxaliplatin (Cayman Chemical; cat. no. 13106) for 24 hours in their respective culture medium.

2.3 Flow cytometry for ecto-CRT and TRAIL-receptors

Subsequent to treatment with doxorubicin or oxaliplatin, cells were harvested using Accutase (Invitrogen™; cat. no. 00-4555-56). Samples were stained in a 96-well U-bottom plate for 30 min at 4 °C with LIVE/DEAD™ Violet stain (1:1,000) followed by primary antibodies for 30 min in PBS and 2% FCS. To quantify the degree of apoptosis, cells were incubated Annexin V-FITC in Annexin V buffer for an additional 20 minutes at room temperature. Flow cytometry was performed on CytoFLEX (Beckman Coulter Life Sciences) and analyzed using FlowJo v10.10.0 (BD, Ashland, OR, USA). Flow cytometry was assessed on gated viable non-apoptotic (Annexin V-negative, DAPI- or LIVE/DEAD™-negative) cells, as shown in Figure A.1.

2.4 Phosphoflow for intracellular p-EIF2α

Subsequent to treatment with doxorubicin or oxaliplatin, cells were harvested using Accutase (Invitrogen™; cat. no. 00-4555-56), washed with PBS and stained with LIVE/DEAD™ Violet stain (1:1,000) for 30 min at 4 °C in a 96-well U-bottom plate. For fixation, BD Cytofix (BD Biosciences; cat. no. 554655) was used at a 1:2 dilution in PBS (final PFA concentration of 2%) and incubated for 15 min at 37 °C. Cells were permeabilized using BD Phosflow™ Perm Buffer III (BD Biosciences; cat. no. 558050) for 30 min at 4 °C followed by intracellular staining of p-EIF2α (for the full list of antibodies, see Table B.1).

2.5 NK cell isolation and siRNA-mediated knockdown of TRAIL

Human NK cells were isolated from Buffy coats obtained from healthy volunteer blood donors at Sahlgrenska University Hospital. Peripheral blood mononuclear cells (PBMCs) were isolated by density gradient centrifugation using Lymphoprep (Stemcell technologies, cat. no. 07861). NK cells were isolated from PBMCs using magnetic bead separation with the human NK cell isolation kit (Miltenyi Biotec, cat. no. 130-092-657) and NK cell purity based on CD56/CD3 staining was confirmed with flow cytometry.

In order to induce surface TRAIL-expression, isolated NK cells at a concentration of $1 \cdot 10^6$ cells/ml were stimulated for 72h with 10 ng/ml recombinant human IL-15 and 500 IU/ml IL-2 in IMDM supplemented with 10% heat-inactivated FCS, 1% penicillin-streptomycin (PeSt, Gibco), 2 mM L-glutamine (Gibco), and 1 mM sodium pyruvate (Gibco). Knockdown of TRAIL-expression was performed by incubating NK cells for another 72 hours with either Accell Human *TNFSF10* siRNA (Dharmacon Reagents) or Accell Non-targeting siRNA #1 as control, in Accell siRNA delivery medium (Horizon Discovery, cat. no. B-005000-100) supplemented with 1% penicillin-streptomycin and containing the same IL-2 and -15 concentrations as in the previous step. The presence and absence of surface TRAIL-expression was confirmed with flow cytometry.

2.6 NK cell functional assays

A total of 50,000 NK cells per well were seeded into 96-well U-bottom plates and pre-incubated with or without NKp46 blocking antibody for 20 min at room temperature. Target cells were treated with doxorubicin or oxaliplatin as previously described, harvested, and labeled with CellTrace™ Violet for 20 minutes at 37 °C. CellTrace™-labeled target cells were then added to NK cells at an effector:target (E:T) ratio of 1:1. Co-cultures were incubated in the presence of anti-human CD107a antibody for 3 h at 37 °C. After incubation, cells were washed with PBS, stained with LIVE/DEAD™ far-red viability dye (1:1,000) for 30 min at 4 °C, and analyzed

by flow cytometry. For degranulation, the percentage of CD107a-positive NK cells was assessed based on the gated live CellTrace™-negative population. For cytotoxicity, the percentage of dead target cells (LIVE/DEAD™-positive) was assessed based on the gated CellTrace™-positive population. In some experiments, target cells were also pre-incubated with blocking antibody to CRT (ab2907) at a dilution of 1:100 for 20 min at room temperature before coculture.

2.7 Protein folding prediction

Three-dimensional protein structure prediction was performed using AlphaFold3 and Boltz-2 on the AlphaFold Server and Tamarind Bio server, respectively [21][22][23] using the amino acid sequences of NKp46 (Uniprot O76036, aa 22-214 (extracellular domain), or 1-304 (full-length)), TRAIL (Uniprot P50591, aa 35-281), TRAIL-R1 (Uniprot, O00220, aa 118-239), TRAIL-R2 (Uniprot 14763, aa 56-183), and CRT (Uniprot Q96L12, aa 1-417). Predicted structures were downloaded in PDB or mmCIF format for further analysis.

2.8 Protein interaction analysis and residue scanning

All structures were imported into and analyzed using Maestro v14.5 (Schrödinger, LLC, New York, NY, USA). Prior to analysis, protein preparation was performed using the Protein Preparation Wizard to assign bond orders, add hydrogen atoms, generate appropriate protonation states, optimize the hydrogen-bonding network, and minimize the structures using the OPLS4 force field. Protein interaction analysis (PIA) was performed to identify interface residues at the NKp46–TRAIL binding surface. Residues were classified as interacting if any atom of the residue was located within 4 Å of an atom belonging to the binding partner. Interface residues were identified for both NKp46 and TRAIL.

To identify residues influencing the interaction between NKp46 and TRAIL, an initial alanine-scanning analysis was performed using the MM-GBSA Residue Scanning module (Fig. 2.1). Here, interacting residues at the NKp46-TRAIL interface were individually mutated to alanine using side-chain prediction with backbone minimization, and residues within 5 Å of the mutation site were included in the local refinement. Mutations were evaluated based on the predicted change in binding free energy (ΔAffinity, or more commonly $\Delta\Delta G$). Residues for which alanine substitution increased the binding free energy ($\Delta\Delta G > 2$) were interpreted as contributing favorably to the interaction (so-called "hotspots").

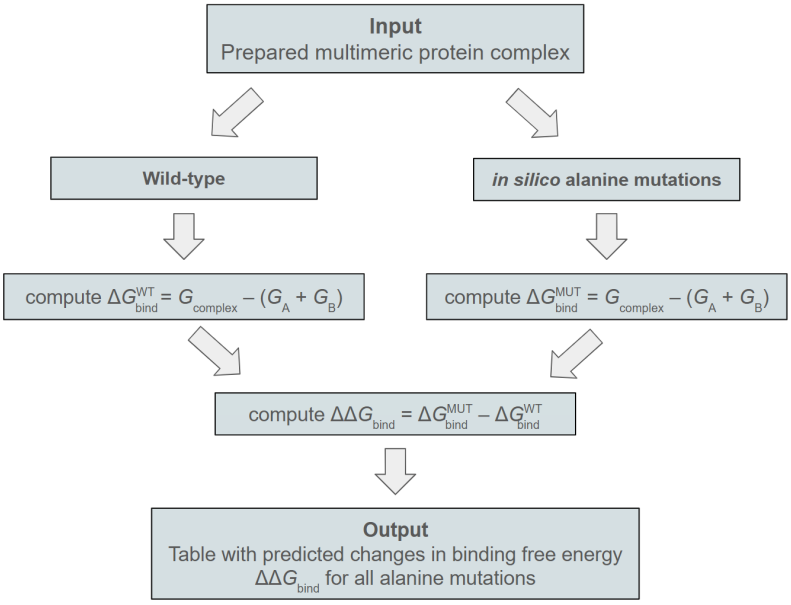

Figure 2.1: Flow chart describing the process of computational alanine scanning at an overall level. Briefly, the input is a set of PDB coordinates for the protein complex. Prior to analysis, the complex is prepared according to protocol **??**. Selected residues are individually mutated to alanine *in silico* and ΔG_{bind} of the mutated complex is estimated and subsequently compared to theΔG_{bind} of the wild-type complex. The output is a table with predicted changes in binding free energies for all alanine mutations.

2.9 Estimation of binding free energy using Prime MM-GBSA

Residue scanning uses a simplified energy model and evaluates mutations in a largely static structural context. Therefore, for the subset of promising variants, Prime MM-GBSA was subsequently applied to obtain a more detailed and physically rigorous estimate of binding free energy. Prime MM-GBSA was used to estimate the binding free energy of the wild-type and mutant NKp46-TRAIL complexes and to quantify the effect of each substitution on binding affinity. This analysis followed the generation of structural models for all mutants (Section 2.8), ensuring that each variant was evaluated using an identical computational protocol. All calculations were performed using the OPLS4 force field and the VSGB implicit solvation model. For all calculations, the non-mutated binding partners were designated as the receptor, while the mutated chain was treated as the ligand. This assignment was kept constant across all variants to ensure that $\Delta\Delta G_{\text{bind}}$ values reflected only the energetic consequences of the mutation. Local relaxation was performed using Prime's Minimize sampling method. Only residues at directly the ligand interface were allowed to move during minimization to capture local side-chain adjustments at the interface. The same flexible-residue definition was applied to all systems.

The predicted binding energies, calculated as

$$\Delta G_{\text{bind}} = G_{\text{complex}} - (G_{\text{TRAIL}} + G_{\text{Nkp46}}) \tag{2.1}$$

were evaluated in order find the change in binding free energy between the mutated and the wild-type complex according to equation 2.2

$$\Delta\Delta G_{\text{bind}} = \Delta G_{\text{bind}}^{\text{MUT}} - \Delta G_{\text{bind}}^{\text{WT}} \tag{2.2}$$

to assess the impact of each substitution on NKp46-TRAIL binding. Negative $\Delta\Delta G_{\text{bind}}$ values indicate improved binding relative to the wild type.

2.10 Statistical analysis

Data were represented as mean and comparisons were made using paired t-tests or one-way analysis of variance (ANOVA) where applicable. All statistical analyses were conducted using Graphpad Prism v11.0 (Graphpad Software, Inc., La Jolla, CA, USA). P-values <0.05 were considered statistically significant.

3

Results

This chapter is divided into two sections corresponding to the main experimental and computational aims of the study (see Section 1.3). The first section addresses whether TRAIL and TRAIL receptors contribute to NKp46-mediated cytotoxicity and how this contribution is influenced by ER stress-induced changes in target cells, with a particular focus on calreticulin and TRAIL receptor upregulation. The second section investigates the structural basis of the NKp46–TRAIL interaction using *in silico* modelling approaches, including structure prediction, interface analysis, and energetic profiling of key binding residues.

3.1 The role of TRAIL and TRAIL-receptors in NKp46-mediated recognition of ER-stressed cancer cells

NKp46 has previously been reported to bind externalized calreticulin (ecto-CRT) on ER-stressed cancer cells [8], while more recent evidence suggests that it also recognizes TRAIL receptors through *in cis* interaction with TRAIL expressed on NK cells. These observations have led to two partly distinct models of NKp46-mediated target recognition during immunogenic cell death. In this context, the present study investigated the relative contributions of ecto-CRT and TRAIL/TRAIL receptors to NKp46-dependent recognition of cancer cells undergoing ER stress.

3.1.1 TRAIL-R2 and ecto-CRT are co-upregulated on choriocarcinoma cells in response to oxaliplatin treatment

To examine to which extent CRT, and TRAIL-R1/2 are upregulated on cancer cells in response to ER stress, human choriocarcinoma JEG-3 cells were treated with 100 µM oxaliplatin for 24 hours (Fig. 3.1). Oxaliplatin treatment induced ER stress and activation of PERK as measured by increased intracellular levels of p-eIF2α (Fig. 3.1a). TRAIL-receptors and ecto-CRT were also upregulated in response to treatment (Fig. 3.1b) and stratification of the cell population based on ecto-CRT expression revealed that cells exhibiting high ecto-CRT (ecto-CRT$^{\text{high}}$) also displayed increased surface levels of TRAIL-R2 compared with ecto-CRT$^{\text{low}}$ cells (Fig. 3.2). These findings reveal that upregulation of ecto-CRT is associated with concomitant upregulation of TRAIL-R2 also at the single-cell level. This co-expression suggests that, in addition to ecto-CRT, increased TRAIL receptor expression may represent a potential contributing factor to NKp46-dependent degranulation observed under conditions of ER stress and immunogenic cell death.

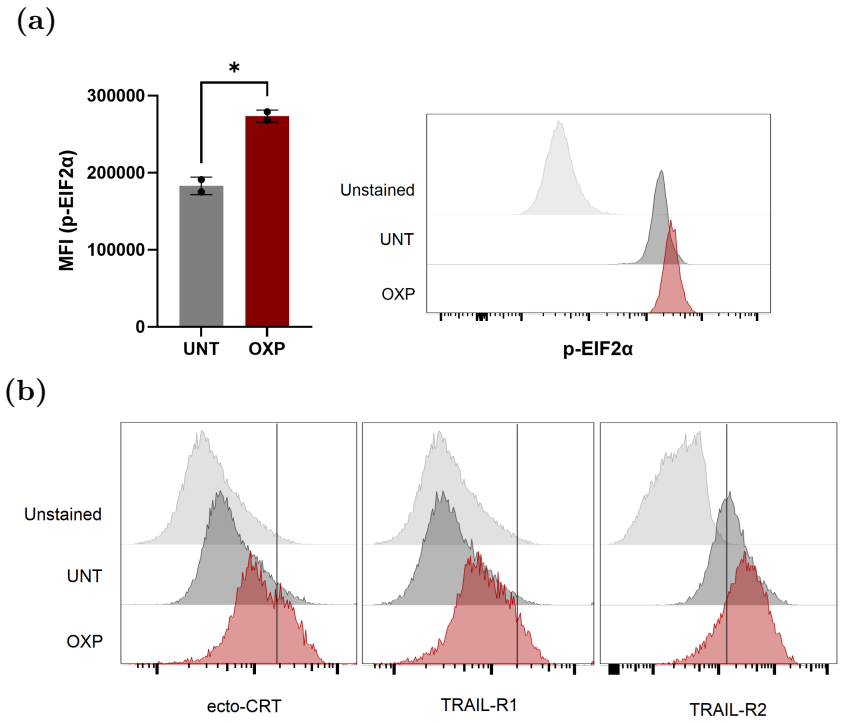

Figure 3.1: Oxaliplatin induces phosphorylation of eIF2α and upregulation of ecto-CRT and TRAIL receptors. (a) Median fluorescence intensity (left) and representative flow cytometry histograms (right) of p-EIF2α. (b) Representative flow cytometry plots of ecto-CRT, TRAIL-R1, and TRAIL-R2. Human choriocarcinoma JEG-3 cells were treated with 100 µM oxaliplatin for 24 hours and p-eIF2α was quantified with phosphoflow and the remaining markers with regular flow cytometry ($n = 2$).

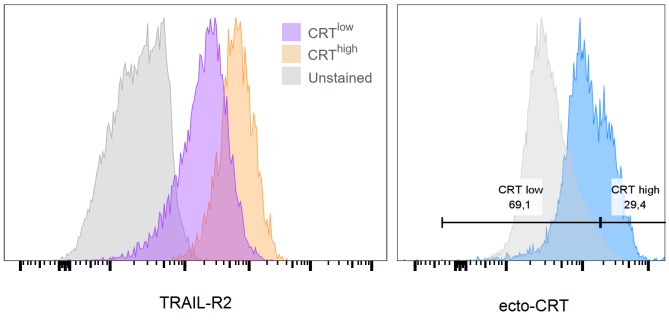

Figure 3.2: TRAIL-R2 and ecto-CRT are co-upregulated on JEG-3 cells in response to oxalipltain-treatment. Left: Flow cytometry histogram of TRAIL-R2 surface expression in oxaliplatin-treated cells gated as CRT^{low} or CRT^{high} according to the gating strategy shown in the right panel.

3.1.2 TRAIL is required for NKp46-mediated NK cell cytotoxicity against oxaliplatin- and daunorubicin-treated cells

To determine whether TRAIL contributes to NKp46-mediated cytotoxicity against JEG-3 cells, stimulated NK cells were transfected with either anti-*TNFSF10* (TRAIL)

siRNA to reduce TRAIL expression or a non-targeting control siRNA (Fig. 3.3). Degranulation after cocuture with JEG-3 cells was then assessed in the presence or absence of NKp46 blockade (aNKp46). The percentages of degranulating (CD107a-positive) NK cells are shown in Figure 3.4. As expected, NK cells degranulated in response to JEG-3 cells, whereas both NKp46 blockade and *TNFSF10* knockdown reduced degranulation compared with control conditions. Moreover, the protective effect of NKp46 blockade was almost completely lost when TRAIL was absent, and vice versa, reinforcing that TRAIL is required for NKp46-mediated cytotoxicity. Interestingly, NK-cell degranulation was lower against oxaliplatin-treated than untreated JEG-3 cells (see supplementary Fig. A.2a) and Annexin V/DAPI staining revealed that a substantial fraction of oxaliplatin-treated JEG-3 cells were in early or late apoptosis. Exposure of phosphatidylserine (PtdSer) on the cell surface has been shown to inhibit NK cell signaling via TIM-3, which may partly explain the reduced degranulation observed against oxaliplatin-treated cells [24]. Nevertheless, the overall response pattern remained similar, with both NKp46 blockade and *TNFSF10* knockdown significantly reducing NK-cell degranulation against oxaliplatin-treated targets.

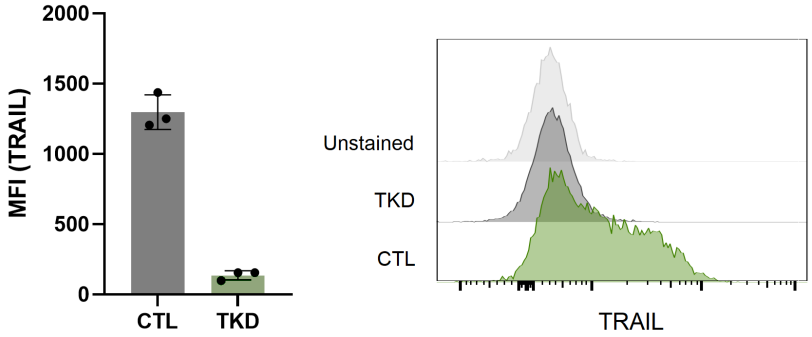

Figure 3.3: Mean fluorescence intensity (MFI) of TRAIL (left) and representative flow cytometry plots of TRAIL (right). NK cells were stimulated with IL-2 and IL-15 for 3 days followed by transfection with either non-targeting (CTL) or anti-*TNFSF10* (TRAIL) siRNA (TKD) $n = 3$).

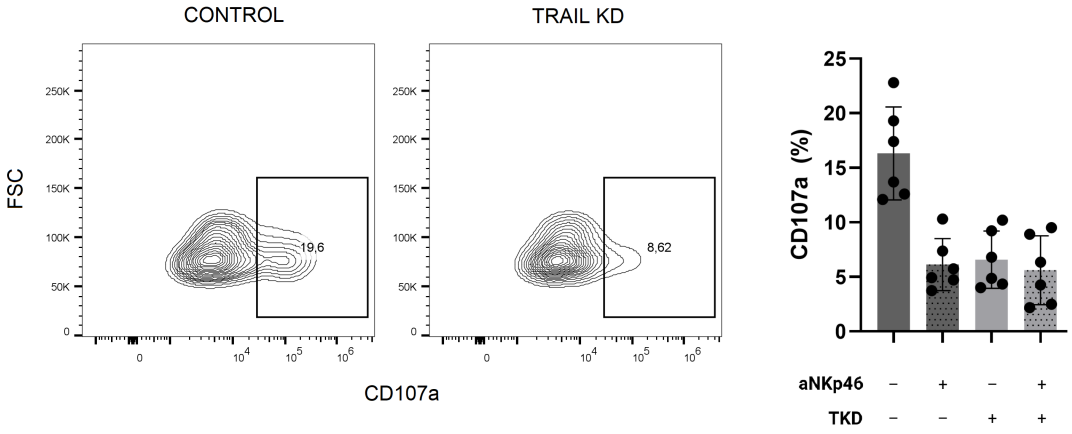

Figure 3.4: Representative flow cytometry plots (left) and percentage of degranulating NK cells isolated from the blood of six healthy donors (right), as measured by surface CD107a, in response to untreated JEG-3 cells (E:T ratio 1:1, 3 h coculture).

In an attempt to induce pre-apoptotic features of ER stress, JEG-3 cells were instead treated with the ICD-drug daunorubicin. As shown in Figure 3.5, ecto-CRT expression did not change in response to daunorubicin-treatment. However, there was an approximate 5-fold increase in surface expression of TRAIL-R2.

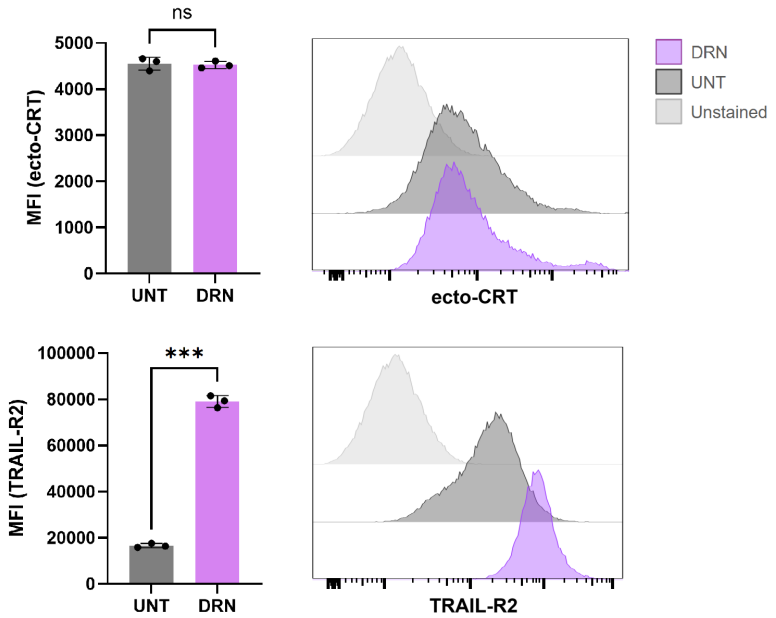

Figure 3.5: Daunorubicin induces upregulation of TRAIL-R2 but not ecto-CRT on JEG-3 cells. JEG-3 cells were treated with 1 uM daunorubicin for 24 hours and surface expression of ecto-CRT and TRAIL-R2 was measured with flow cytometry ($n = 3$).

To investigate whether the observed upregulation of TRAIL-R2 contributes to enhanced NK-cell degranulation, a degranulation assay was performed using daunorubicin-

treated target cells. NK cells exhibited a substantial increase in degranulation in response to treatment, indicating enhanced susceptibility of the target cells to NK-cell recognition (Fig. 3.6). However, this increase was not completely abolished by NKp46 blockade, which accounted for approximately 40% of the treatment-induced effect. These findings indicate that, although NKp46 contributes significantly to the enhanced degranulation response, additional activating receptor–ligand interactions are likely involved. While ligands for NKG2D, such as MICA/B and ULBPs, were not directly assessed in this study, their potential contribution is plausible, as they are stress-inducible molecules that are upregulated by DNA damage responses, ER stress, oxidative stress, and other forms of cellular stress [25]. Nevertheless, a consistent pattern was observed across conditions: the inhibitory effect of NKp46 blockade was largely lost when TRAIL was absent, in agreement with previous results and supporting a central role for the NKp46–TRAIL axis in mediating NK-cell responses to treated and untreated cancer cells.

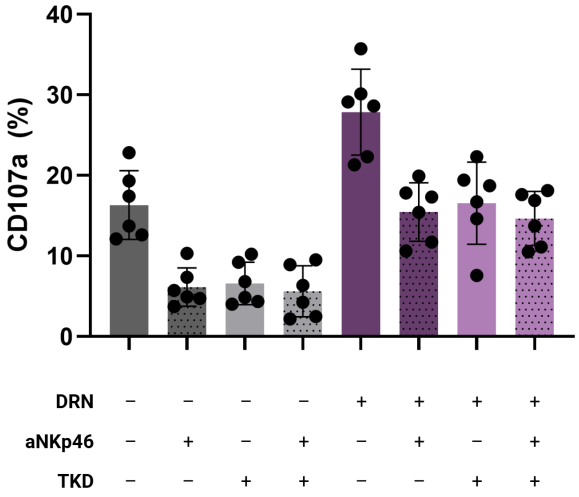

Figure 3.6: Percentage of degranulating NK cells isolated from the blood of six healthy donors, as measured by surface CD107a, in response to untreated (grey) and daunorubicin-treated (purple) JEG-3 cells (E:T ratio 1:1, 3 h coculture).

3.1.3 Ecto-CRT and TRAIL-R2 are upregulated in response to doxorubicin treatment in MDA-MB-231 and A549 cells

To determine whether additional human cancer cell lines exhibit a similar response to induction of ICD, MDA-MB-231 (breast adenocarcinoma) and A549 (lung carcinoma) were treated with 2 µM doxorubicin for 24 hours (Fig. 3.7). As observed with oxaliplatin, doxorubicin induced ER stress and activation of the PERK pathway, as indicated by increased phosphorylation of intracellular eIF2α (Fig. 3.7). Doxorubicin treatment also resulted in significant upregulation of both ecto-CRT and TRAIL-R2 across both MDA-MB-231 and A549 (Fig. 3.7). However, the magnitude of TRAIL-R2 upregulation was significantly lower than that observed in JEG-3 cells, most likely because MDA-MB-231 and A549 already express high levels of TRAIL-R2 at baseline.

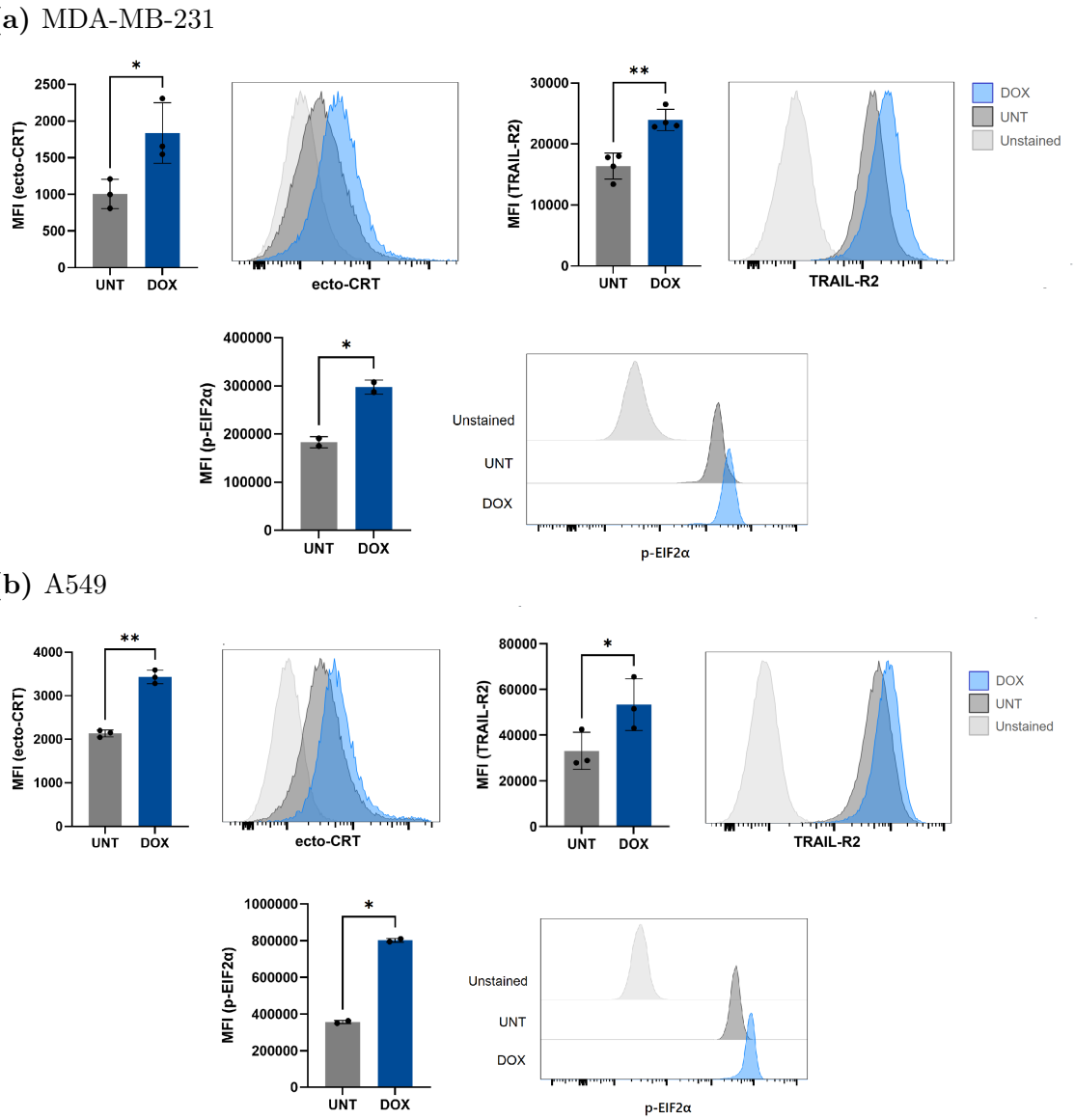

Figure 3.7: Median fluorescence intensity (MFI) and representative histograms for ecto-CRT (top left), TRAIL-R (top right), and p-eIF2α (bottom) of MDA-MB-231 (a) and A549 (b). in MDA-MB-231 (a) and A549 (b) cells. Cells were treated with 2 µM doxorubicin (DOX) for 24 h or left untreated, and analysed by flow cytometry (n = 3-4). For p-eIF2α, phosphoflow was performed on fixed and permeabilized cells (n = 2). Statistics were performed using a paired t-test (*P<0.05, **P<0.01).

3.1.4 TRAIL knockdown, but not CRT blockade, impairs NKp46-mediated degranulation

To investigate whether the concomitant upregulation of ecto-CRT and TRAIL-R2 enhances NK-cell degranulation, and to determine whether ecto-CRT or TRAIL is the principal mediator of this interaction, degranulation assays were performed using NK cells co-cultured with untreated or doxorubicin-treated MDA-MB-231 cells (Fig. 3.8). Assays were conducted in the presence or absence of NKp46 blockade and

with NK cells transfected with either control or anti-*TNFSF10* siRNA. In addition, a subset of target cells was pre-incubated with an anti-CRT antibody prior to co-culture.

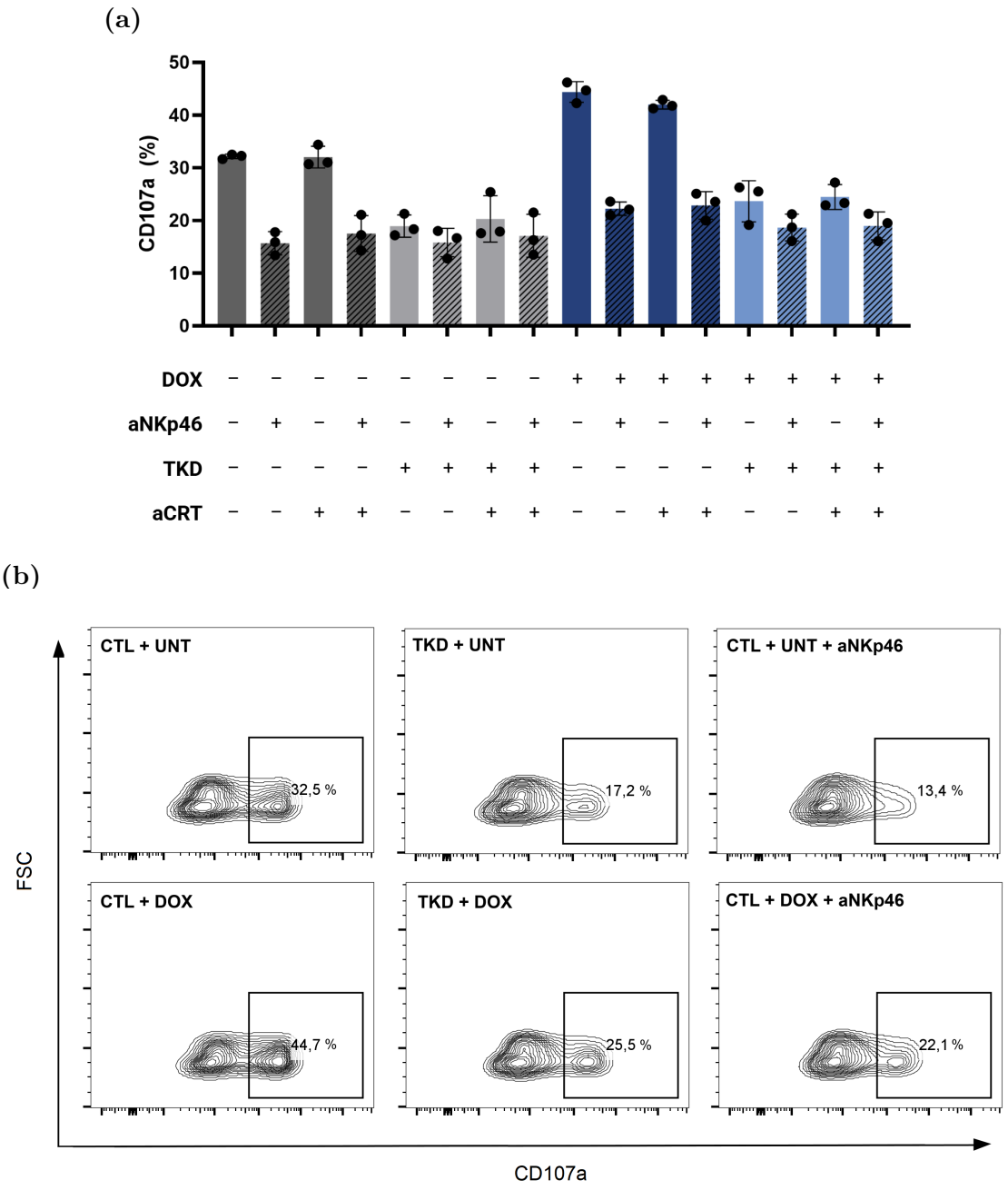

Figure 3.8: (a) Percentage of degranulating NK cells isolated from the blood of three healthy donors, as measured by surface CD107a, in response to untreated (grey) and doxorubicin-treated (blue) MDA-MB-231 (E:T ratio 1:1, 3 h coculture). (b) Representative flow cytometry plots of NK cells (TKD or CTL) against untreated and doxorubicin-treated cells. TKD = TRAIL knockdown, CTL = control, UNT = untreated, DOX = Doxorubicin.

As shown in Figure 3.8, NK cells degranulated significantly more against doxorubicin-treated than untreated MDA-MB-231 cells under control conditions, i.e., in the absence of both NKp46 blockade and *TNFSF10* knockdown. Notably, this increase was largely abrogated by NKp46 blockade and *TNFSF10* knockdown, indicating that NKp46 and TRAIL predominantly mediates the enhanced degranulation induced by doxorubicin treatment. Consistent with the results obtained in JEG-3, the inhibitory effect of NKp46 blockade on degranulation against both untreated and doxorubicin-treated target cells was largely lost following *TNFSF10* knockdown, suggesting that TRAIL is required for efficient NKp46-mediated target recognition.

Interestingly, although ecto-CRT was expressed on both untreated and doxorubicin-treated MDA-MB-231 cells and was further upregulated following treatment (see Fig. 3.7), CRT blockade did not significantly reduce NK-cell degranulation under any of the tested conditions. Instead, the enhanced NK-cell activity observed following doxorubicin treatment appears to be more closely associated with increased TRAIL receptor expression (Fig. 3.7). Notably, NKp46 blockade did not completely abolish the increase in degranulation induced by doxorubicin treatment, suggesting that, although the enhanced response is largely mediated through NKp46, additional stress-induced ligands or signaling pathways may also contribute to NK-cell activation following ER stress. A similar degranulation assay was also performed using A549 cells (Fig. A.3) and consistent with the previous results, it also shows a functional interdependence between NKp46 and TRAIL, whereas blockade of ecto-CRT had no discernible effect on NK-cell degranulation.

3.2 AI-based structure prediction and molecular modelling of TRAIL-NKp46 interactions

In this part of the project, the three-dimensional structure of the NKp46–TRAIL complex was predicted using deep-learning-based structure prediction, followed by *in silico* mutagenesis to find important interacting residues and evaluate whether some interface residues could be modified to improve binding affinity. This analysis was motivated by the functional data suggesting a key role for the NKp46–TRAIL axis in NK-cell recognition. However, as no experimentally resolved structure of the NKp46–TRAIL interaction currently exists, computational modelling was used to gain insight into the putative binding interface and to identify residues that may contribute to complex stability and affinity

3.2.1 AlphaFold predicts a C3-symmetric NKp46 arrangement around a TRAIL trimer

TRAIL and other ligands of the TNF family are known trimerize in the cell membrane [26] and it is therefore plausible to assume that also within the NKp46-TRAIL complex, one or several copies of NKp46 interact with a TRAIL trimer. Indeed, at a 1:1 NKp46:TRAIL ratio, AlphaFold predicts a NKp46-TRAIL complex with a TRAIL-trimer in the center surrounded by three monomers of NKp46 as shown in

Figure 3.9. Protein interaction analysis found 86 interacting residues for a total of 101 interactions in each NKp46-TRAIL interface. More specifically, the D2 domain and the hinge-region of each NKp46 molecule interacts with the distal part of one TRAIL molecule. In addition, the D1 domain of the same NKp46 molecule also interacts with the membrane-proximal part of another TRAIL molecule (see Figure 3.10). The AlphaFold ipTM and pTM scores for this model are 0.48 and 0.52, respectively, indicating limited confidence in the overall assembly of the complex. The predicted aligned error (PAE) matrix is shown in Figure 3.11. Inspection of the PAE plot reveals some uncertainty in the relative positining of the three NKp46 monomers with respect to the central TRAIL trimer, as well as in their positioning relative to one another. In contrast, the PAE values within each individual NKp46 monomer are low, indicating high confidence in their internal folds. Similarly, the TRAIL trimer itself (particularly the trimeric head region) exhibits low PAE between TRAIL monomers, consistent with a well-defined and confidently predicted trimeric structure. This suggests that while AlphaFold predicts the monomeric structures and the TRAIL trimer with high confidence, the relative arrangement of NKp46 molecules around the TRAIL trimer remains uncertain.

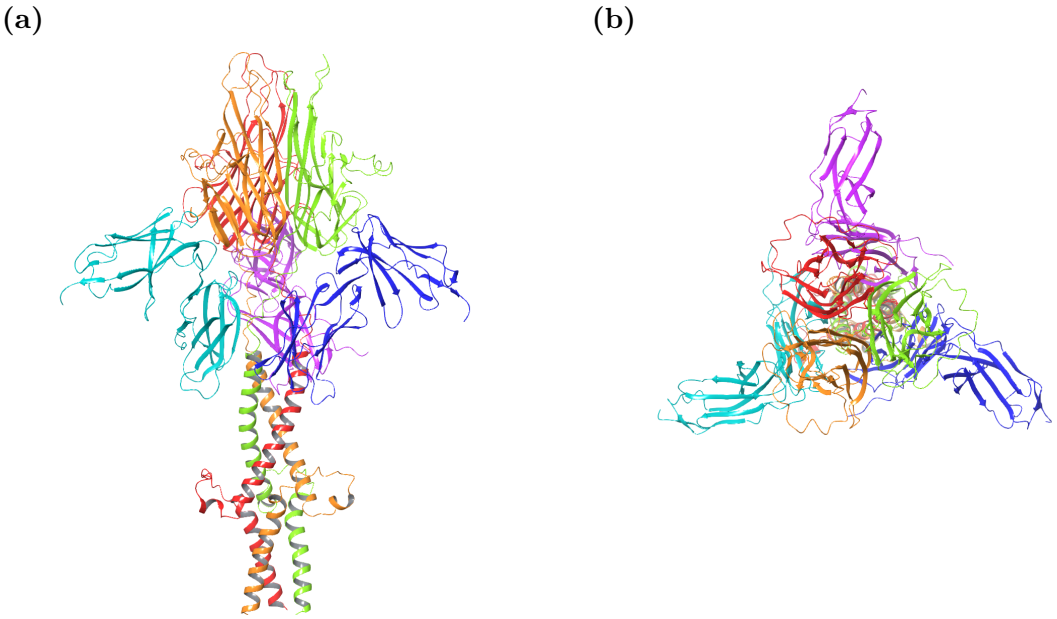

Figure 3.9: AlphaFold3-predicted structure of one TRAIL-trimer in the center surrounded by three copies of the extracellular portion of NKp46 as viewed from the side (a) and from the top (b). The structure was generated using the amino acid sequence of NKp46 (Uniprot O76036, aa 22-214) and TRAIL (Uniprot P50591, aa 35-281) and the corresponding PAE matrix is shown in Figure 3.11.

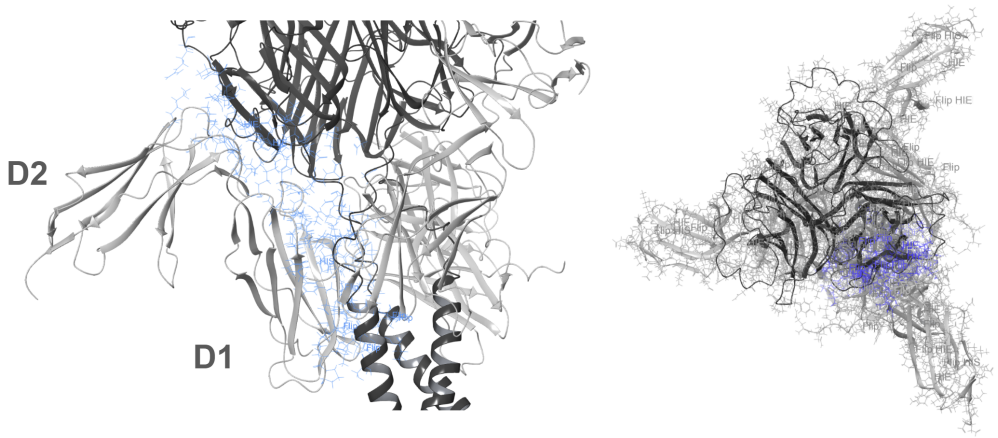

Figure 3.10: The D2 domain and the interdomain hinge of NKp46 (grey) interacts with the distal part of one TRAIL (black) molecule, while the D1 domain interacts with the membrane-proximal part of another TRAIL molecule. All 86 interface residues are shown in blue. For clarity, only one of the three interfaces are shown.

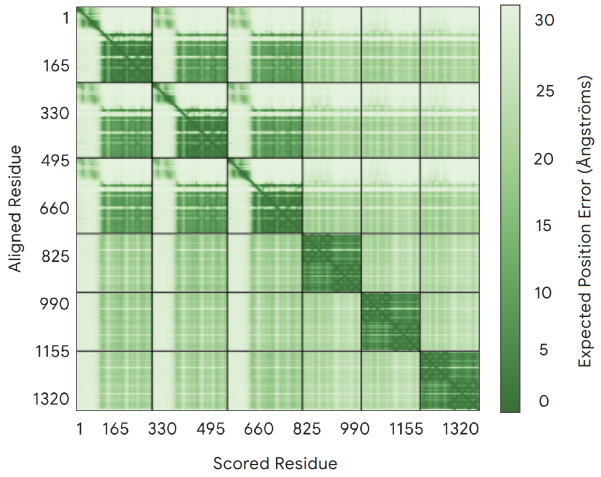

Figure 3.11: Predicted aligned error (PAE) matrix for the AlphaFold-predicted NKp46–TRAIL complex. The first three diagonal blocks (upper left) correspond to the three TRAIL monomers, while the last three diagonal blocks correspond to the three NKp46 chains. Low PAE values within individual diagonal blocks indicate high confidence in the internal structures of each monomer and in the TRAIL trimeric assembly. In contrast, elevated PAE values between TRAIL and NKp46 blocks, as well as between NKp46 chains, indicate uncertainty in their relative positioning.

3.2.2 Computational alanine scanning identifies key residues contributing to stabilization of the NKp46–TRAIL interface

Because the AlphaFold-predicted NKp46 monomer structures exhibited relatively high PAE between NKp46 and the TRAIL trimer, a direct application of alanine scanning on a single predicted structure was considered insufficient for robust iden-

tification of interaction hotspots. Instead, an ensemble-based approach was employed, in which multiple independent AlphaFold predictions were generated to sample conformational variability. Computational alanine scanning was then performed on each individual model, in which the NKp46-TRAIL-interacting residues on NKp46 were individually mutated to alanine and calculated for the change in local binding free energy, and the results were integrated to identify consensus hotspot residues. Residues consistently identified across the structural ensemble were prioritized, thereby increasing confidence in the predicted functional interface despite local structural uncertainty in the monomer models.

The top consensus hotspots and their averaged $\Delta\Delta G$ values are shown in Table 3.1 and Figure 3.12. Higher $\Delta\Delta G$ values indicate a greater predicted loss of binding affinity opon alanine substitution and, consequently, a larger contribution of the wild-type residue to complex stability. These results suggest that several residues make substantial stabilizing contributions to the NKp46–TRAIL interface. Among the predicted hotspots, Tyr 100 in the NKp46 D2 domain exhibited the largest average $\Delta\Delta G$ value. Structural analysis revealed that Tyr 100 interacts with residues in the distal region of TRAIL and forms a hydrogen bond with TRAIL Glu 218 (Fig. 3.13)), identifying this interaction as a key electrostatic anchor at the interface. To further validate this prediction, Prime MM-GBSA calculations were performed on the Tyr100Ala mutant complex, revealing an approximately 26 kcal/mol increase in binding free energy (ΔG_{bind}) relative to the wild-type complex, consistent with a strongly destabilizing mutation.

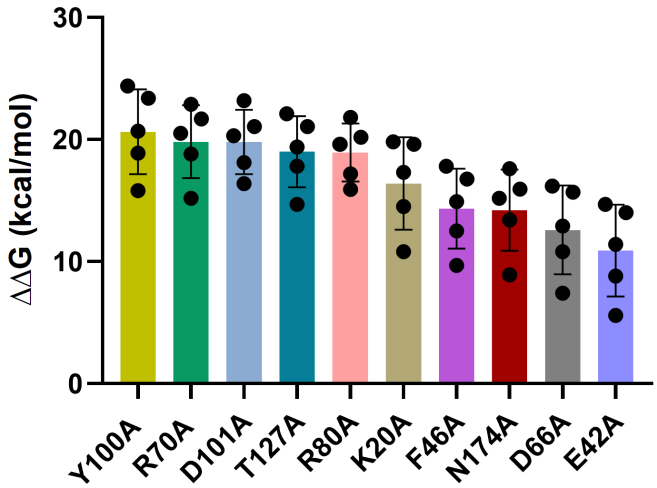

Figure 3.12: Predicted effects of alanine substitutions on protein–protein binding affinity. Bars represent the mean change in binding free energy ($\Delta\Delta G$, kcal/mol) calculated by Prime MM-GBSA residue scanning for each alanine mutation across five independent AlphaFold-generated complex models. Higher $\Delta\Delta G$ values indicate a greater predicted loss of binding affinity and therefore a larger contribution of the wild-type residue to complex stability. Numerical values are presented in Table 3.1

Interacting residue	$\Delta\Delta G$ (kcal/mol)	Interacting residue	$\Delta\Delta G$ (kcal/mol)
NKp46 Tyr 100	20.64	NKp46 Lys 20	16.40
NKp46 Arg 70	19.82	NKp46 Phe 46	14.33
NKp46 Asp 101	19.81	NKp46 Asn 174	14.21
NKp46 Thr 127	19.01	NKp46 Asp 66	12.60
NKp46 Arg 80	18.94	NKp46 Glu 42	10.90

Table 3.1: Predicted effects of alanine substitutions on protein–protein binding affinity. Values are mean change in binding free energy ($\Delta\Delta G$, kcal/mol) calculated by Prime MM-GBSA residue scanning for each alanine mutation across five independent AlphaFold-generated complex models. Higher $\Delta\Delta G$ values indicate a greater predicted loss of binding affinity and therefore a larger contribution of the wild-type residue to complex stability.

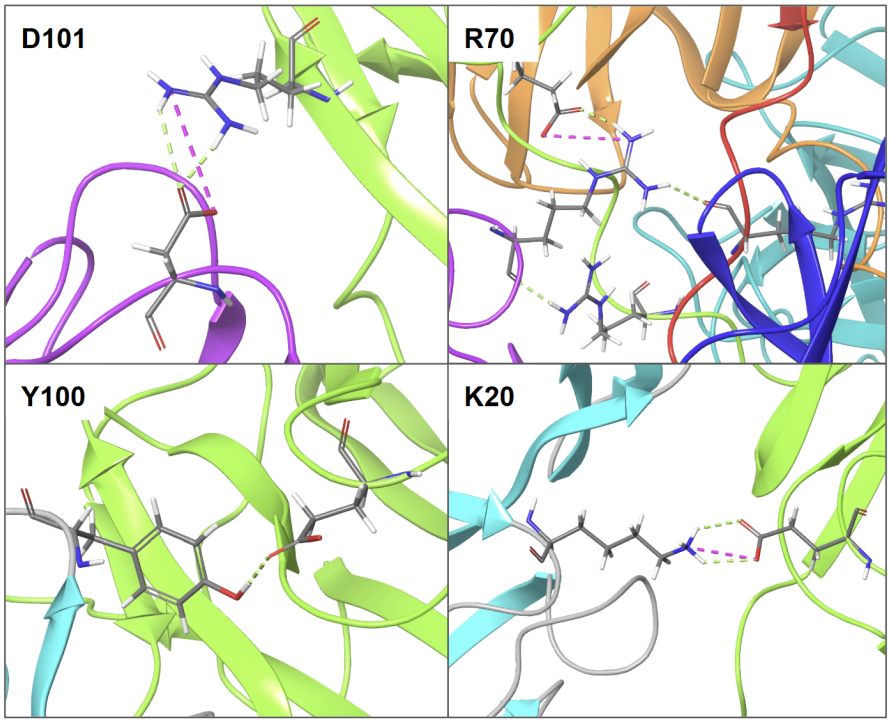

Figure 3.13: Structural context of the NKp46–TRAIL interface centered on NKp46 Asp101 interacting with TRAIL Arg 136 through two hydrogen bonds and a salt bridge (a), NKp46 Arg 70 interacting with TRAIL Arg 83 on both TRAIL molecules via hydrogen bonding and with Glu 144 via both hydrogen bonding and a salt bridge (b), NKp46 Tyr 100 engaging TRAIL Glu 218 with one hydrogen bond (c), and NKp46 Lys 20 interacting with TRAIL Glu 218 through two hydrogen bonds and one salt bridge (d). Hydrogen bonds: lime-green dashed lines. Salt bridges: purple dashed lines).

Arg 70 was also consistently identified as a hotspot across all alanine scanning calculations. As shown in Figure 3.13, Arg 70 forms two hydrogen bonds with TRAIL Arg 83, one on the distal TRAIL monomer and one on the membrane-proximal monomer. In addition, it forms both a salt bridge and a hydrogen bond with TRAIL Glu 144, providing a structural explanation for its substantial energetic

contribution to complex stability. Similarly, to assess the energetic importance of this residue, Prime MM-GBSA calculations were performed on the Arg70Ala mutant complex, revealing an approximately 28 kcal/mol increase in binding free energy relative to the wild-type complex. This result is in good agreement with the alanine scanning prediction and further supports the role of Arg 70 as a key contributor to NKp46–TRAIL binding.

4

Discussion

In the current study, it was shown that calreticulin and TRAIL-receptors, particularly TRAIL-R2, are co-upregulated in response to immunogenic cell death (ICD)-inducing treatment such as oxaliplatin and doxorubicin. The concomitant increase in TRAIL receptor expression may provide a mechanistic link that reconciles two previously distinct models of NKp46-mediated target recognition, one involving direct binding of NKp46 to ecto-CRT and another involving recognition of TRAIL-receptors via *in cis* NKp46-TRAIL binding.

The present data demonstrate that TRAIL is required for NKp46-mediated degranulation against both untreated and daunorubicin-treated JEG-3 choriocarcinoma cells, as well as doxorubicin-treated MDA-MB-231 breast adenocarcinoma cells. Notably, the doxorubicin-induced increase in NK-cell degranulation appeared to be largely driven by activation of the NKp46–TRAIL axis, as both NKp46 blockade and *TNFSF10* (TRAIL) knockdown abolished approximately 60% of the enhanced response. Furthermore, the inhibitory effect of NKp46 blockade was almost completely lost following *TNFSF10* knockdown regardless of whether anthracycline-treated cells were used. Together, these findings support a model in which TRAIL is required for efficient NKp46-mediated recognition and killing of both untreated and ER-stressed cancer cells. In contrast, blockade of ecto-CRT on MDA-MB-231 cells did not significantly reduce NK-cell degranulation, despite a measurable increase in surface CRT expression following doxorubicin treatment. Instead, the concomitant increase in TRAIL-R2 expression provides a more likely explanation for the enhanced NKp46-dependent response observed following treatment. These findings suggest that increased sensitivity to NK-cell recognition following ER stress is primarily associated with increased expression of TRAIL receptors rather than increased exposure of ecto-CRT. Importantly, NKp46-dependent degranulation was observed not only against ER-stressed target cells but also against untreated cells. This observation is difficult to reconcile with a model in which ecto-CRT serves as the primary NKp46 ligand, as CRT exposure is typically associated with ER stress and immunogenic cell death. While ecto-CRT may contribute to NKp46-mediated recognition under specific conditions, additional ligands are required to explain the broader role of NKp46 in cancer cell recognition. The present data suggest that TRAIL receptors constitute one such ligand system.

However, these results do not imply that NKp46 does not bind to ecto-CRT at all. In fact, NKp46 is constituively expressed on resting NK cells, while TRAIL is not. Consequently, NKp46-dependent cytotoxicity mediated by resting NK cells against ER-stressed cancer cells could plausibly rely to a greater extent on ecto-CRT

recognition. Nevertheless, CRT blockade failed to reduce degranulation even when TRAIL expression was reduced by *TNFSF10* knockdown, suggesting that ecto-CRT contributed little, if at all, to the responses measured under the experimental conditions used in this study. The discrepancy between the present findings and those reported by Sen santara et al. [8] may have several explanations. In their study, ecto-CRT was identified as a ligand for NKp46 and ER-stressed cancer cells were shown to induce enhanced degranulation of unstimulated NK cells. In contrast, CRT blockade did not significantly reduce NK-cell degranulation under any of the conditions tested in the present study. Several methodological and biological differences between the studies may account for these apparently divergent findings. First, the extent of CRT externalization following ICD is highly cell-type dependent, and many cancer cell lines exhibit only modest or inconsistent ecto-CRT exposure. Although doxorubicin treatment significantly increased CRT expression in MDA-MB-231 cells, the magnitude of this increase was relatively limited. It is therefore possible that higher levels of ecto-CRT expression would have resulted in a more pronounced contribution to NK-cell activation.

Second, differences in experimental design may have influenced the observed outcomes. All degranulation assays in the present study were performed at a fixed effector-to-target ratio of 1:1, whereas Sen Santara et al. used an effector-to-target ratio of 1:3 when assessing degranulation induced by ER stressed cancer cells [8]. If the interaction between NKp46 and CRT is intrinsically weak, increasing the number of ecto-CRT-expressing target cells would increase the cumulative opportunity for receptor engagement and may therefore be required to observe a measurable functional effect. Under such conditions, even a low-affinity interaction could contribute detectably to NK-cell activation, whereas the same interaction may have little impact at lower target-cell densities. This interpretation is consistent with reported binding affinities, as the interaction between NKp46 and CRT has been estimated to be approximately three orders of magnitude weaker than the interaction between TRAIL and its receptors [8][19]. Consequently, under conditions in which TRAIL is expressed, TRAIL-mediated interactions would be expected to dominate NKp46-dependent target recognition. Finally, the exclusive use of stimulated NK cells in the present study likely contributed to the generally high levels of degranulation observed across conditions and may also account for differences relative to studies using unstimulated NK cells. Collectively, these findings do not argue against a role for ecto-CRT in NKp46 biology. Rather, they suggest that under conditions where TRAIL is present, recognition of TRAIL receptors through the NKp46–TRAIL axis constitutes the dominant mechanism underlying NKp46-dependent cytotoxicity, including during ER stress.

One limitation of the present study is that the functional analyses relied primarily on NK-cell degranulation as a readout of cytotoxic activity. Although CD107a expression is a well-established marker of NK-cell activation and correlates with cytotoxic potential, it does not directly measure target-cell death. Consequently, the observed effects of NKp46 blockade and *TNFSF10* knockdown cannot be assumed to translate quantitatively into differences in cancer cell killing. Additional experiments using direct cytotoxicity assays, such as viability measurements, or chromium-release

assays, would further strengthen the conclusions and provide a more comprehensive assessment of the contribution of the NKp46–TRAIL axis to tumor-cell elimination.

The computational alanine scanning identified several residues that are predicted to contribute substantially to the stability of the NKp46–TRAIL interface, with Tyr 100 and Arg 70 emerging as the most consistent hotspot residues across all five AlphaFold-generated complex models. Structural inspection revealed that both residues participate in multiple hydrogen-bonding and electrostatic interactions with TRAIL, providing a plausible molecular explanation for their large predicted energetic contributions. Despite these promising findings, the results should be interpreted with caution. The overall confidence of the AlphaFold-predicted NKp46–TRAIL complex is relatively low, particularly at the protein–protein interface, and the calculated binding energies are highly dependent on the accuracy of the predicted structure. Computational alanine scanning and MM-GBSA calculations are best viewed as hypothesis-generating tools rather than definitive evidence of energetic hotspots. Consequently, the identified residues should be considered candidates for future experimental validation rather than confirmed determinants of binding.

An encouraging observation is that Tyr 100 and Arg 70 were consistently identified as hotspot residues across five independently generated AlphaFold models. While the predicted binding poses exhibit some variability, the repeated identification of these residues suggests that their importance is relatively robust to structural uncertainty. This consensus provides greater confidence than any individual prediction alone and highlights these positions as attractive targets for rational protein engineering. From a protein design perspective, introducing mutations in NKp46 is likely more straightforward than modifying TRAIL. TRAIL forms a homotrimer, and residues at the receptor-binding interface may also contribute to trimer assembly or structural stability. Mutations designed to improve NKp46 binding could therefore inadvertently destabilize the TRAIL trimer or alter its biological function. Nevertheless, systematic mutagenesis of TRAIL remains an interesting direction for future work, as it may identify substitutions that strengthen receptor binding while preserving trimer stability.

The relatively low confidence observed in the membrane-proximal region of the complex is also consistent with known limitations of AlphaFold. The model is predominantly trained on experimentally determined protein structures, the majority of which originate from X-ray crystallography. Membrane proteins and membrane-associated complexes are substantially underrepresented in these datasets because they are inherently difficult to crystallize and characterize structurally. As a result, AlphaFold generally performs best for well-defined globular domains and often exhibits lower confidence for flexible loops, membrane-proximal regions, and dynamic protein interfaces [21]. The reduced confidence in these regions of the NKp46–TRAIL complex is therefore not unexpected and further emphasizes the need for experimental validation. Future studies could combine these computational predictions with site-directed mutagenesis and quantitative binding assays, such as surface plasmon resonance or biolayer interferometry, to validate the predicted hotspot residues experimentally. In addition, molecular dynamics simulations

could provide further insight into the conformational flexibility of the interface and assess whether the identified interactions remain stable over time. Together, such approaches would provide a more comprehensive understanding of the NKp46–TRAIL interaction and support the rational engineering of receptor variants with improved binding properties.

4.1 Conclusion

In brief, the present findings demonstrate that TRAIL is required for NKp46-mediated degranulation against ER-stressed cancer cells. Doxorubicin treatment increased surface expression of both ecto-CRT and TRAIL-R2 on MDA-MB-231 cells. However, blocking calreticulin did not significantly reduce degranulation. These findings suggest that, under the conditions investigated, the enhanced NKp46-mediated degranulation is primarily driven by the interaction of TRAIL with TRAIL receptors on the target cells rather than by ecto-CRT.

Furthermore, iterative alanine-scanning analyses of five independent AlphaFold models identified Tyr100 and Arg70 as the residues predicted to contribute most strongly to stabilization of the NKp46–TRAIL interface. Further characterization and validation of this interaction may provide a basis for optimizing NKp46–TRAIL binding and for evaluating the therapeutic potential of the NKp46–TRAIL axis in cancer.

References

[1] E. O. Long, H. S. Kim, D. Liu, M. E. Peterson, and S. Rajagopalan, "Controlling natural killer cell responses: Integration of signals for activation and inhibition," *Annual Review of Immunology*, vol. 31, pp. 227–258, Volume 31, 2013 Mar. 2013, ISSN: 07320582. DOI: 10.1146/ANNUREV-IMMUNOL-020711-075005/CITE/REFWORKS. [Online]. Available: https://www.annualreviews.org/content/journals/10.1146/annurev-immunol-020711-075005.

[2] I. Prager et al., "Nk cells switch from granzyme b to death receptor–mediated cytotoxicity during serial killing," *The Journal of Experimental Medicine*, vol. 216, p. 2113, 9 Sep. 2019, ISSN: 15409538. DOI: 10.1084/JEM.20181454. [Online]. Available: https://pmc.ncbi.nlm.nih.gov/articles/PMC6719417/.

[3] M. Vitale et al., "Nkp44, a novel triggering surface molecule specifically expressed by activated natural killer cells, is involved in non–major histocompatibility complex–restricted tumor cell lysis," *The Journal of Experimental Medicine*, vol. 187, p. 2065, 12 Jun. 1998, ISSN: 00221007. DOI: 10.1084/JEM.187.12.2065. [Online]. Available: https://pmc.ncbi.nlm.nih.gov/articles/PMC2212362/.

[4] A. D. Barrow, C. J. Martin, and M. Colonna, "The natural cytotoxicity receptors in health and disease," *Frontiers in Immunology*, vol. 10, p. 451 720, MAY May 2019, ISSN: 16643224. DOI: 10.3389/FIMMU.2019.00909/FULL. [Online]. Available: www.frontiersin.org.

[5] C. E. Foster, M. Colonna, and P. D. Sun, "Crystal structure of the human natural killer (nk) cell activating receptor nkp46 reveals structural relationship to other leukocyte receptor complex immunoreceptors," *Journal of Biological Chemistry*, vol. 278, pp. 46 081–46 086, 46 Nov. 2003, ISSN: 0021-9258. DOI: 10.1074/JBC.M308491200. [Online]. Available: https://www.sciencedirect.com/science/article/pii/S0021925820823771#fig3.

[6] K. Takahashi, K. Takeda, I. Saiki, T. Irimura, and Y. Hayakawa, "Functional roles of tumor necrosis factor-related apoptosis-inducing ligand-dr5 interaction in b16f10 cells by activating the nuclear factor-b pathway to induce metastatic potential," *Cancer science*, vol. 104, pp. 558–562, 5 May 2013, ISSN: 1349-7006. DOI: 10.1111/CAS.12112. [Online]. Available: https://pubmed.ncbi.nlm.nih.gov/23347256/.

[7] S. Sivori et al., "Nkp46 is the major triggering receptor involved in the natural cytotoxicity of fresh or cultured human nk cells. correlation between surface density of nkp46 and natural cytotoxicity against autologous, allogeneic or xenogeneic target cells," *European Journal of Immunology*, vol. 29, pp. 1656–1666, 5 May 1999, ISSN: 0014-2980. DOI: 10.1002/(SICI)1521-4141(199905)29:05<1656::AID-IMMU1656>3.0.CO;2-1.

[8] S. S. Santara et al., "The nk-cell receptor nkp46 recognizes ecto-calreticulin on er-stressed cells," *Nature 2023 616:7956*, vol. 616, pp. 348–356, 7956 Apr. 2023,

ISSN: 1476-4687. DOI: 10.1038/s41586-023-05912-0. [Online]. Available: https://www.nature.com/articles/s41586-023-05912-0.

[9] A. V. Schadewijk, E. F. V. Wout, J. Stolk, and P. S. Hiemstra, "A quantitative method for detection of spliced x-box binding protein-1 (xbp1) mrna as a measure of endoplasmic reticulum (er) stress," *Cell Stress and Chaperones*, vol. 17, pp. 275–279, 2 Mar. 2012, ISSN: 1355-8145. DOI: 10.1007/S12192-011-0306-2. [Online]. Available: https://www.sciencedirect.com/science/article/pii/S1355814523011264?via%3Dihub.

[10] X. Chen and J. R. Cubillos-Ruiz, "Endoplasmic reticulum stress signals in the tumour and its microenvironment," *Nature Reviews Cancer 2020 21:2*, vol. 21, pp. 71–88, 2 Nov. 2020, ISSN: 1474-1768. DOI: 10.1038/s41568-020-00312-2. [Online]. Available: https://www.nature.com/articles/s41568-020-00312-2.

[11] G. D. Conza and P. C. Ho, "Er stress responses: An emerging modulator for innate immunity," *Cells 2020, Vol. 9, Page 695*, vol. 9, p. 695, 3 Mar. 2020, ISSN: 2073-4409. DOI: 10.3390/CELLS9030695. [Online]. Available: https://www.mdpi.com/2073-4409/9/3/695/htm%20https://www.mdpi.com/2073-4409/9/3/695.

[12] N. Casares et al., "Caspase-dependent immunogenicity of doxorubicin-induced tumor cell death," *The Journal of experimental medicine*, vol. 202, pp. 1691–1701, 12 2005. DOI: 10.1084/jem.20050915. [Online]. Available: www.jem.org/cgi/doi/10.1084/jem.20050915.

[13] O. Kepp et al., "Crosstalk between er stress and immunogenic cell death," *Cytokine & Growth Factor Reviews*, vol. 24, pp. 311–318, 4 Aug. 2013, ISSN: 1359-6101. DOI: 10.1016/J.CYTOGFR.2013.05.001. [Online]. Available: https://www.sciencedirect.com/science/article/pii/S1359610113000415?via%3Dihub.

[14] J. Fucikova, R. Spisek, G. Kroemer, and L. Galluzzi, "Calreticulin and cancer," *Cell Research*, vol. 31, p. 5, 1 Jan. 2020, ISSN: 17487838. DOI: 10.1038/S41422-020-0383-9. [Online]. Available: https://pmc.ncbi.nlm.nih.gov/articles/PMC7853084/.

[15] A. Blees et al., "Structure of the human mhc-i peptide-loading complex," *Nature*, vol. 551, pp. 525–528, 7681 Nov. 2017, ISSN: 1476-4687. DOI: 10.1038/NATURE24627. [Online]. Available: https://pubmed.ncbi.nlm.nih.gov/29107940/.

[16] "Mechanisms of pre-apoptotic calreticulin exposure in immunogenic cell death," *EMBO Journal*, vol. 28, pp. 578–590, 5 Mar. 2009, ISSN: 02614189. DOI: 10.1038/EMBOJ.2009.1/FIGURES/7. [Online]. Available: https://link.springer.com/article/10.1038/emboj.2009.1.

[17] O. Kepp et al., "Eif2 phosphorylation as a biomarker of immunogenic cell death," *Seminars in Cancer Biology*, vol. 33, pp. 86–92, Aug. 2015, ISSN: 10963650. DOI: 10.1016/j.semcancer.2015.02.004. [Online]. Available: https://pubmed.ncbi.nlm.nih.gov/25749194/%20https://pubmed.ncbi.nlm.nih.gov/25749194/?utm_source=chatgpt.com.

[18] S. Qian et al., "Advancements in the study of the immune molecule nkp46 in immune system-related diseases," *Clinical Reviews in Allergy & Immunology*

2024 67:1, vol. 67, pp. 96–110, 1 Nov. 2024, ISSN: 1559-0267. DOI: 10.1007/S12016-024-09010-5. [Online]. Available: https://link.springer.com/article/10.1007/s12016-024-09010-5.

[19] A. Truneh et al., "Temperature-sensitive differential affinity of trail for its receptors. dr5 is the highest affinity receptor," *The Journal of biological chemistry*, vol. 275, pp. 23 319–23 325, 30 Jul. 2000, ISSN: 0021-9258. DOI: 10.1074/JBC.M910438199. [Online]. Available: https://pubmed.ncbi.nlm.nih.gov/10770955/.

[20] M. de Bruyn, V. R. Wiersma, W. Helfrich, P. Eggleton, and E. Bremer, "The ever-expanding immunomodulatory role of calreticulin in cancer immunity," *Frontiers in Oncology*, vol. 5, p. 129 866, FEB Feb. 2015, ISSN: 2234943X. DOI: 10.3389/FONC.2015.00035/BIBTEX. [Online]. Available: www.frontiersin.org.

[21] "Addendum: Accurate structure prediction of biomolecular interactions with alphafold 3," *Nature*, vol. 636, E4, 8042 Dec. 2024, ISSN: 14764687. DOI: 10.1038/S41586-024-08416-7;TECHMETA. [Online]. Available: https://www.nature.com/articles/s41586-024-08416-7.

[22] J. Wohlwend et al., "Boltz-1 democratizing biomolecular interaction modeling," *bioRxiv*, p. 2024.11.19.624167, Dec. 2025, ISSN: 2692-8205. DOI: 10.1101/2024.11.19.624167. [Online]. Available: https://pmc.ncbi.nlm.nih.gov/articles/PMC11601547/.

[23] Tamarind Bio, *State of the art computational tools for biology*, https://www.tamarind.bio/, Accessed: 2026-05-27, 2025.

[24] L. Kristenson et al., "Deletion of the tmem30a gene enables leukemic cell evasion of nk cell cytotoxicity," *Proceedings of the National Academy of Sciences of the United States of America*, vol. 121, e2316447121, 15 Apr. 2024, ISSN: 10916490. DOI: 10.1073/PNAS.2316447121;ISSUE:ISSUE:DOI. [Online]. Available: /doi/pdf/10.1073/pnas.2316447121?download=true.

[25] G. Tan, K. M. Spillane, and J. Maher, "The role and regulation of the nkg2d/nkg2d ligand system in cancer," *Biology*, vol. 12, p. 1079, 8 Aug. 2023, ISSN: 20797737. DOI: 10.3390/BIOLOGY12081079. [Online]. Available: https://pmc.ncbi.nlm.nih.gov/articles/PMC10452210/.

[26] É. S. Vanamee and D. L. Faustman, "On the trail of better therapies: Understanding tnfrsf structure-function," *Cells 2020, Vol. 9, Page 764*, vol. 9, p. 764, 3 Mar. 2020, ISSN: 2073-4409. DOI: 10.3390/CELLS9030764. [Online]. Available: https://www.mdpi.com/2073-4409/9/3/764/htm%20https://www.mdpi.com/2073-4409/9/3/764.

A

Supplementary Figures

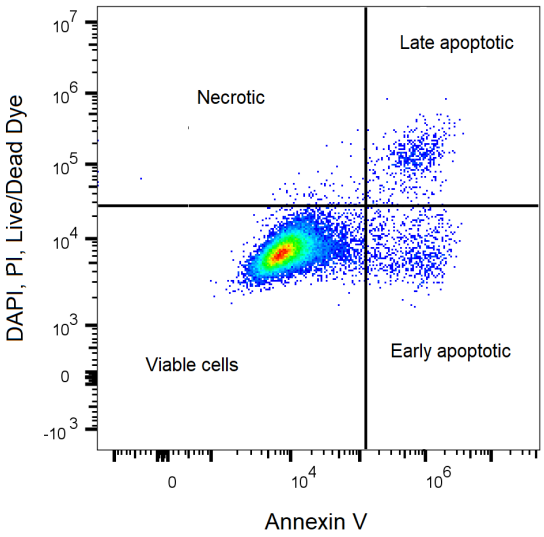

Figure A.1: Defined populations based on Annexin V and staining with viability dye. Following antibody staining, cells were incubated with Annexin V-FITC for 20 minutes at room temp in Annexin V buffer.

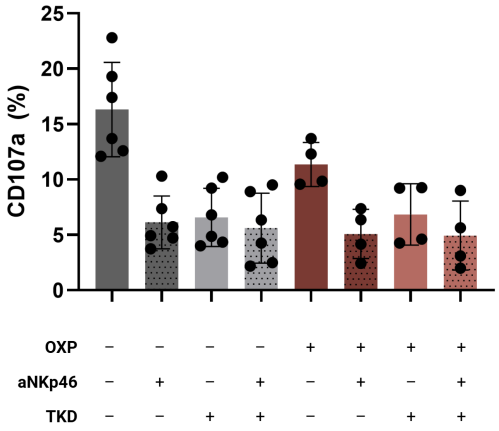

Figure A.2: Percentage of degranulating NK cells isolated from the blood of six healthy donors, as measured by surface CD107a, in response to untreated and oxaliplatin-treated JEG-3 cells (3 h coculture, E:T ratio 1:1).

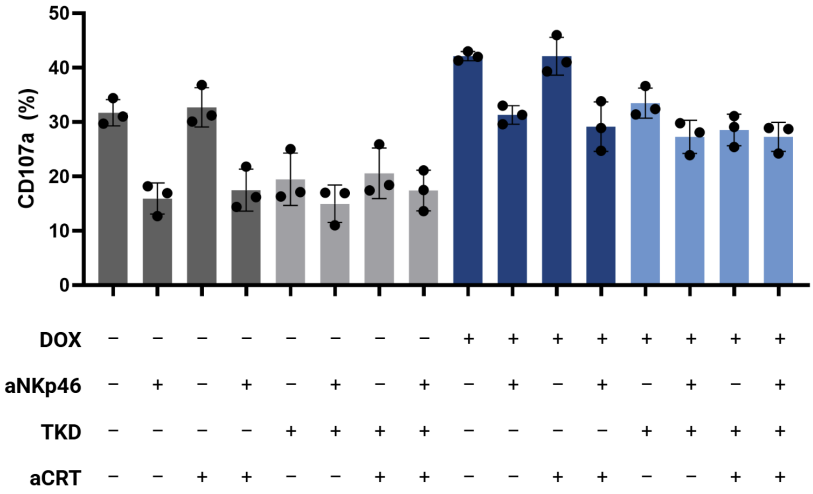

Figure A.3: Percentage of degranulating NK cells isolated from the blood of three healthy donors, as measured by surface CD107a, in response to untreated and doxorubicin-treated A549 cells (3 h coculture, E:T ratio 1:1).

B

Supplementary Tables

Table B.1: Antibodies and viability dyes used in the experiments.

Reagent	Clone	Reference	Dilution
Viability dye / Cell stain			
LIVE/DEAD™ Fixable Violet Dead Cell Stain		ThermoFisher (Cat# L34955)	1:1000
LIVE/DEAD™ Fixable Near IR (780) Viability Kit		ThermoFisher (Cat# L34994)	1:1000
LIVE/DEAD™ Fixable Far Red Dead Cell Stain Kit		ThermoFisher (Cat# L34973)	1:1000
CellTrace™ Violet Cell Proliferation Kit		ThermoFisher (Cat# C34557)	1:1000
Annexin V-FITC		BD Biosciences (Cat# 560931)	1:1000
Antibody			
PE anti-human CRT	FMC75	Abcam (Cat# ab83220)	1:100
APC anti-human CRT	681233	Abcam (Cat# FAB38981A)	1:100
PE anti-human TRAIL-R1	S35-934	BD Biosciences (Cat# 564180)	1:20
APC anti-human TRAIL-R2	B-K29	BD Biosciences (Cat# 565498)	1:20
Anti-human NKp46	KL247	Prof. Silvia Parolini	1:2
PE anti-human TRAIL	RIK-2	Thermo Fisher (Cat# 12-9927-42)	1:20
PE-Cy7 anti-human CD107a	H4A3	BD Biosciences (Cat# 561348)	1:20
CoraLite® Plus 488 p-eIF2S1 (Ser51)	1A4A11	Thermo Fisher CL488-68023	1:50

DEPARTMENT OF SOME SUBJECT OR TECHNOLOGY
CHALMERS UNIVERSITY OF TECHNOLOGY
Gothenburg, Sweden
www.chalmers.se

CHALMERS
UNIVERSITY OF TECHNOLOGY